Key Points:
- We confirm the viability of transient maria outgassed atmosphere for pressures from 1 to 10 mbar
- Three-dimensional simulations demonstrate where volatile deposition may occur
- Atmospheric escape and outgassing chemistry play important roles

Supporting Information:
- Supporting Information S1

Correspondence to:
I. Aleinov,
Igor.Aleinov@nasa.gov

Modeling a Transient Secondary Paleolunar Atmosphere: 3-D Simulations and Analysis

I. Aleinov[1,2], M. J. Way[2,3,4], C. Harman[2,5], K. Tsigaridis[1,2], E. T. Wolf[6], and G. Gronoff[7,8]

[1]Center for Climate Systems Research, Columbia University, New York, NY, USA, [2]NASA Goddard Institute for Space Studies, New York, NY, USA, [3]Theoretical Astrophysics, Department of Physics and Astronomy, Uppsala University, Uppsala, Sweden, [4]GSFC Sellers Exoplanet Environments Collaboration, Greenbelt, MD, USA, [5]Department of Applied Physics and Applied Mathematics, Columbia University, New York, NY, USA, [6]Laboratory for Atmospheric and Space Physics, University of Colorado Boulder, Boulder, CO, USA, [7]Science Directorate, Chemistry and Dynamics Branch, NASA Langley Research Center, Hampton, VA, USA, [8]SSAI, Hampton, VA, USA

Abstract The lunar history of water deposition, loss, and transport postaccretion has become an important consideration in relation to the possibility of a human outpost on the Moon. Very recent work has shown that a secondary primordial atmosphere of up to 10 mbar could have been emplaced $\sim 3.5 \times 10^9$ years ago due to volcanic outgassing from the maria. Using a zero-dimensional chemistry model, we demonstrate the temperature dependence of the resulting major atmospheric components (CO or CO_2). We use a three-dimensional general circulation model to test the viability of such an atmosphere and derive its climatological characteristics. Based on these results, we then conjecture on its capability to transport volatiles outgassed from the maria to the permanently shadowed regions at the poles. Our preliminary results demonstrate that atmospheres as low as 1 mbar are viable and that permanent cold trapping of volatiles is only possible at the poles.

1. Introduction

The Moon has had a number of relatively short-lived atmospheres. Soon after its formation it is likely to have had a 1000–2500 K lunar magma ocean (LMO). The initial primordial lunar atmosphere was formed as a result of outgassing from the LMO. Work by Stern (1999) claimed this SiO_2-dominated atmosphere could have been as thick as present-day Venus′ atmosphere with a scale height of order 75 km. More recent work by Saxena et al. (2017) state that it was a metal-dominated atmosphere (with SiO_2 vapor being present for only ~100 years after the formation) of 1–100 mbar on the warm side and collapsing on the cold far side of the planet. Such an atmosphere would have been short-lived and collapsed completely once the LMO had a crystallized crust. According to Saxena et al. (2017) the crystallization would have happened in ~1,000 years, while complete solidification of the LMO could have taken up to 10–100 Myr (Elkins-Tanton et al., 2011; Nemchin et al., 2009). Stern (1999) postulated a second epoch in which mare volcanism gave rise to a thin atmosphere punctuated by a "high-mass" collisionally supported atmosphere of order 10^{-5} mbar for very short periods of time. Other research (Prem et al., 2015; Stewart et al., 2011) also suggest that a thin transient atmosphere could have been formed by volatile-rich impacts. For the rest of its history the Moon's atmosphere was an exceedingly thin exosphere, which currently measures $\sim 10^{-12}$ mbar (Benna et al., 2015; Cook et al., 2013; Stern, 1999).

More recent research by Needham and Kring (2017; hereafter NK2017) explores in detail the second epoch mentioned above. The longevity of this short-term high-mass atmosphere would be controlled by a competition between outgassing from the maria and atmospheric escape. According to NK2017 most of the outgassing from lunar maria occurred between 3.8×10^9 and 3.1×10^9 years ago (Ga) and at its peak it could sustain an atmosphere of ~10 mbar for ~70 million years. Such an atmosphere would be similar in thickness to that of modern Mars and could play a major role in transporting volatiles from the maria to the poles. In turn these volatiles could be trapped in permanently shadowed regions (PSR) or buried under the regolithic dust.

We have expanded the study of NK2017 by first looking at results from a zero-dimensional (0-D) chemistry model to determine the atmosphere's major constituents based on the species outgassed from the maria. We

then use these constituents as input to a three-dimensional (3-D) general circulation model (GCM) (Way et al., 2017) to better understand the temperature structure of this hypothetical atmosphere. We hope to eventually use such 3-D simulations to better understand volatile transport, deposition, and, ultimately, volatile distributions on the Moon.

In section 2 we discuss the importance of chemistry in determining the possible composition of the transient atmosphere. In section 3 we explore some of the nuances of atmospheric escape. Section 4 outlines how the 3-D GCM was set up, and section 5 describes the results and some of the broader implications.

2. Chemical Composition of the Lunar Atmosphere

As described by NK2017 the volcanic gases entering the atmosphere from the maria were predominantly CO, H_2O, sulfur (S), and H_2. However, much of the water vapor would be subject to condensation soon after eruption, as determined by the surface temperature. Atomic S is not a conventionally volatile species (e.g., Kasting et al., 1989), and other studies have suggested that sulfur would outgas as S_2, much as it does on Io (e.g., Zolotov & Fegley Jr, 1999), and as H_2S (Renggli et al., 2017). Additionally, elemental sulfur rapidly polymerizes to form aerosol molecules and has a negligible saturation vapor pressure for the temperatures shown here (Harman et al., 2018; Lyons, 2008). Given that the S flux is comparable to the flux of CO, removing some or most of the S as a secondary species or aerosol would reduce the mass of the atmosphere, leaving CO and H_2 as the predominant contributors to the lunar atmosphere (Renggli et al., 2017). We can take this one step further and introduce the fluxes of volcanic gases into a box model for atmospheric chemistry (not shown, but it is based on the reducing chemistry scheme seen in Harman et al., 2015), assuming a range of temperatures potentially relevant to the Moon and the appropriate solar spectrum for a ∼600-Myr-old Sun (Claire et al., 2012). Initial tests at 10 mbar suggest that the predominant species in the lunar atmosphere at steady state are dependent upon the temperature, with low temperatures ($\lesssim$150 K) preserving CO from conversion to CO_2 via chemical interaction with water vapor photolysis products (namely, OH), and modest temperatures ($\gtrsim$175 K) conversely promoting a CO_2-dominated atmosphere. This is a known phenomenon for cold CO_2-dominated atmospheres (Gao et al., 2015; Zahnle et al., 2008). We have not interactively resolved the chemistry in the 3-D model but have instead chosen to simulate two end-member scenarios where the atmosphere is either primarily CO or CO_2. However, it is important to note that while the conversion between CO and CO_2 is mediated largely by OH, a source of oxygen is also necessary. This oxygen could be produced through the loss of hydrogen to space (derived from water vapor photolysis; see section 3).

3. Atmospheric Loss Processes

Thermal escape from a modest lunar atmosphere could substantially modify not only the chemical composition but potentially the total atmospheric mass if escape rates are large enough. NK2017 suggest thermal escape rates on the order of 10 kg/s based on earlier estimates (Vondrak, 1974; Vondrak et al., 1974). However, the total atmospheric mass of a 10-mbar lunar atmosphere would be ∼ 2×10^{16} kg rather than the ∼ 10^9 kg suggested by Vondrak et al. (1974). This large difference in mass changes the altitude of the exobase and therefore increases the surface across which most of the escape occurs.

There exist several potential limits to the escape flux, but here we focus on escape rates in which H is diffusion limited (see Catling & Kasting, 2017), assuming a CO_2-dominated atmosphere with less abundant lighter gases, such as H_2 and CO, as discussed in section 2. For these calculations, the escape parameter (or Jeans parameter) ($\lambda = \frac{GM_p m}{kT_{exo}(R_p + h_{exo})}$) is useful to evaluate the stability of the atmosphere and indicates the thermal escape regime. Here, M_p is the lunar mass, R_p is the planet radius, h_{exo} is the height of the exobase, m is the mass of the escaping atom or molecule, and T_{exo} is the exospheric temperature. For large values of λ, the atmosphere is hydrostatic, and only molecules with sufficient energy will escape (Jeans escape; Catling & Kasting, 2017). When $\lambda \lesssim$ 2–3, the escape becomes hydrodynamic. Based on estimates for the early Earth, Venus, and Mars, we might expect the early Moon's exosphere to be somewhere between 300–1,000 K if it was CO_2 dominated, and warmer if not (Kulikov et al., 2006, 2007). This is turn suggests that some species may be escaping hydrodynamically.

In Table 1 Jeans escape rates are given for each species as a function of the thermospheric/exospheric temperature at the Moon (Vondrak, 1974) which is affected by a number of factors (Fahr & Shizgal, 1983; Zhang et al., 1993). We assume an isothermal atmosphere, so the exospheric altitude varies with the temperature.

Table 1
Atmospheric Jeans Escape Rates

Species	Exospheric temperature							
	500 K		700 K		1500 K		3000 K	
	Exospheric altitude							
	1,200 km		1,721 km		3,800 km		8,000 km	
	λ	Φ_i	λ	Φ_i	λ	Φ_i	λ	Φ_i
CO_2	17	0.04	10	20	3.11	9.6×10^3	0.9	h
CO	11	7.40	7	340	2	11×10^3	0.5	h
O	6.5	240	4	1.7×10^3	1.1	h	0.32	h
H	0.4	h	0.2	h	0.07	h	0.02	h

Notes. λ = Jeans parameter value. Φ_i = Jeans escape rates in units of kilograms per second. h = full hydrodynamic escape; Jeans computations are not valid.

We consider the exospheric altitude for a CO_2 atmosphere in all cases, with a ground temperature of 250 K and the temperature in the atmosphere equal to the exospheric temperature. We noted hydrodynamic escape conditions with an h; the Jeans computations are not valid in these cases. The values in the table suggest that H and H_2 would escape hydrodynamically (e.g., Tian et al., 2009; Volkov et al., 2011) and potentially drag along heavier species if their quantity in the upper atmosphere were not limited by the photodissociation of H_2O and by diffusion through the lower layers of the atmosphere. It is important to note that these assumptions are pessimistic: The lower atmosphere is more likely to be colder on average, which notably reduces the exospheric altitude and therefore the surface area over which escape occurs, lowering the integrated loss rate. Colder temperatures would also limit the water vapor available to photodissociate.

The rate of supply of light gases to high altitudes (i.e., H, H_2, O, and H_2O) will restrict the escape rate as the heavy background gas (either CO or CO_2) will remain largely hydrostatic (see Catling & Kasting, 2017; also Table 1). Water would be restricted to the lower atmosphere largely by the temperature, as mentioned previously. For a CO-dominated atmosphere, the diffusion limit for H_2 is $\Phi_d \approx 2 \times 10^{10} \times f_{H_{tot}} \cdot cm^{-2} \cdot s^{-1}$, or < 6 kg/s (assuming that CO behaves similarly to N_2 as a background gas), and about 50% higher for a CO_2-dominated atmosphere (Hunten, 1973). The availability of hydrogen-bearing species in the upper atmosphere is represented by the weighted sum of mixing ratios for those species, $f_{H_{tot}}$ (Catling & Kasting, 2017). The diffusion limit is relatively insensitive to temperature (see section 3.2.2 of Zahnle et al., 1990).

An important point from Table 1 is that O can have a large escape rate, even for relatively cold exospheric temperatures. However, such large escape rates are not realistic since O comes from CO_2 or CO dissociation. The dissociation rate of CO and CO_2 as computed by Aeroplanets (Gronoff, Simon Wedlund, Mertens, & Lillis, 2012; Gronoff, Simon Wedlund, Mertens, Barthélemy, et al., 2012; Gronoff et al., 2014) in a young Sun scenario does not reach that magnitude, leading to a dissociation rate-limited scenario that should be investigated further.

Suprathermal (or nonthermal) escape mechanisms include charge exchange, ion pickup, sputtering, and solar wind pickup among other processes (Catling & Kasting, 2017) for nonmagnetized bodies. A magnetized Moon (Tikoo et al., 2017) would have suffered polar wind escape (Garcia-Sage et al., 2017). These loss mechanisms would also contribute to the evolution of the lunar atmosphere by driving off heavier molecules like O, independent (and potentially in excess) of thermal escape (e.g., Airapetian et al., 2017; Hunten, 1982), and could ultimately drive the loss of the residual lunar atmosphere. However, models including both avenues have suggested thermal escape would dominate for Earth-sized planets (Erkaev et al., 2013; Kislyakova et al., 2013), as well as for the Moon (Vondrak et al., 1974). The Moon would also spend some part of its orbit in the Earth's shadow (see section 4.1), which would further reduce the impact of suprathermal escape processes. It is important to note, however, that the Earth's magnetic field would have been compressed by more frequent coronal mass ejections (Airapetian et al., 2015, 2016). As an aside, the early Moon may have experienced a large number of impacts, which could have enhanced atmospheric escape (Zahnle & Catling, 2017); this does not fall neatly into either the thermal or suprathermal loss categories. Since the O loss is limited by the dissociation of CO and CO_2, the suprathermal escape only increases the losses marginally. It is therefore possible to estimate the loss rate of a 700-K thermosphere composed of

99.5% CO_2 and 0.5% O (analogous to the Martian atmosphere) at 30 kg/s. In that case, the outgassing rate from the maria as conjectured by NK2017 is able to compensate for the escape and allows the accumulation of an atmosphere, paralleling the impacts of the Apollo missions (Vondrak, 1992). The main question lies with the ability of the Moon to create an initial collisional atmosphere from an exosphere in these conditions: Io has a much higher creation rate but is not able to accumulate an atmosphere (Koga et al., 2018). Ideally, escape rates should be calculated as the atmosphere builds up, but as mentioned above we assume the atmosphere already exists for our calculations.

4. Model Setup

4.1. Orbital Parameters

The latest research (e.g., Canup, 2004; Halliday, 2008; Herwartz et al., 2014; Lock & Stewart, 2016; Lock et al., 2017) tends to support the canonical hypothesis of the Moon forming ~4.5 Ga as a result of a Mars-sized impactor colliding with a proto-Earth (Hartmann & Davis, 1975), though the hypothesis of multiple impacts has gained popularity in recent years (Rufu et al., 2017).

The ejected material formed a disk that accreted and formed the Moon. The shape of the tidal bulge that formed at the time when the Moon had solidified allows one to obtain an estimate for its distance from the Earth at that time (~14.5 Earth radii; see Crotts, 2014). The time evolution of its orbit to the present value of ~60 Earth radii is less constrained and is still subject to debate. Most research (Webb, 1982; Williams, 1999) suggests that the Moon's orbit was evolving rapidly in its early stages with the Moon-Earth distance ~0.75 of its present-day value (60 Earth radii) ~0.5 Gy after formation, though, according to Siegler et al. (2015), the Moon could have been much closer to Earth (41–34 Earth radii) at the time in question.

Another important aspect of the Moon's orbit that is poorly constrained is its obliquity with respect to the normal to the ecliptic. The current value (∼ 1.5°) is rather small and does not produce much seasonal variation. But as the Moon's orbit evolved with time it could have had much higher values. According to several studies (Ćuk et al., 2016; Siegler et al., 2011; Ward, 1975), while its distance from the Earth was between 30 and 40 Earth radii, the Moon underwent a Cassini state transition where its obliquity could have been as high as 50° .

In our current study we assume that the Moon was at a distance of 45 Earth radii from Earth, which implies a sidereal rotation period of 17.8 modern Earth days. At this distance the obliquity should be close to the modern one of ∼ 1.5°. Hence, for simplicity in our simulations we set it to 0. But we plan to address the effect of nonzero obliquity in future studies.

4.2. The GCM

For our experiments we use ROCKE-3D, a planetary GCM developed at the NASA Goddard Institute for Space Studies (Schmidt et al., 2014; Way et al., 2017; also see supporting information). We use $4° \times 5°$ latitude × longitude resolution (~150-km spatial resolution) and 40 atmospheric layers with the upper boundary at 10^{-4} of the surface pressure (~180- to 330-km atmospheric height in our experiments).

Since we are interested in the period after the Late Heavy Bombardment, corresponding to the period of the most intensive lunar volcanic activity, we assume that the Moon's surface has not undergone significant resurfacing since then. Hence, we use modern observational data to describe its surface. For the Moon's topography we use the Lunar Orbiter Laser Altimeter data set (Barker et al., 2016; https://pds. nasa.gov/ds-view/pds/viewProfile.jsp?dsid=LRO-L-LOLA-4-GDR-V1.0). For the surface albedo we use a high-resolution narrow-band normal albedo data set (Lucey et al., 2014), which we scaled to produce a correct broadband Bond albedo (Buratti et al., 1996) when averaged over the entire surface of the planet. To represent the PSRs, we used the Mazarico et al. (2011) data set. We treat PSRs as a special type of surface which is not exposed to direct solar radiation but in all other respects is similar to the rest of the planet's surface. Since our resolution does not allow us to resolve each PSR individually, PSRs are represented statistically, as fractions of grid cells covered by PSRs. Figure S1 (supporting information) shows the surface topography and PSR fractions on the ROCKE-3D grid. For our resolution the highest PSR fraction is 28.2%, which still allows us to treat PSRs as subregions of the grid cells, redistributing the direct solar radiation inside the cell accordingly.

Table 2
Experiments

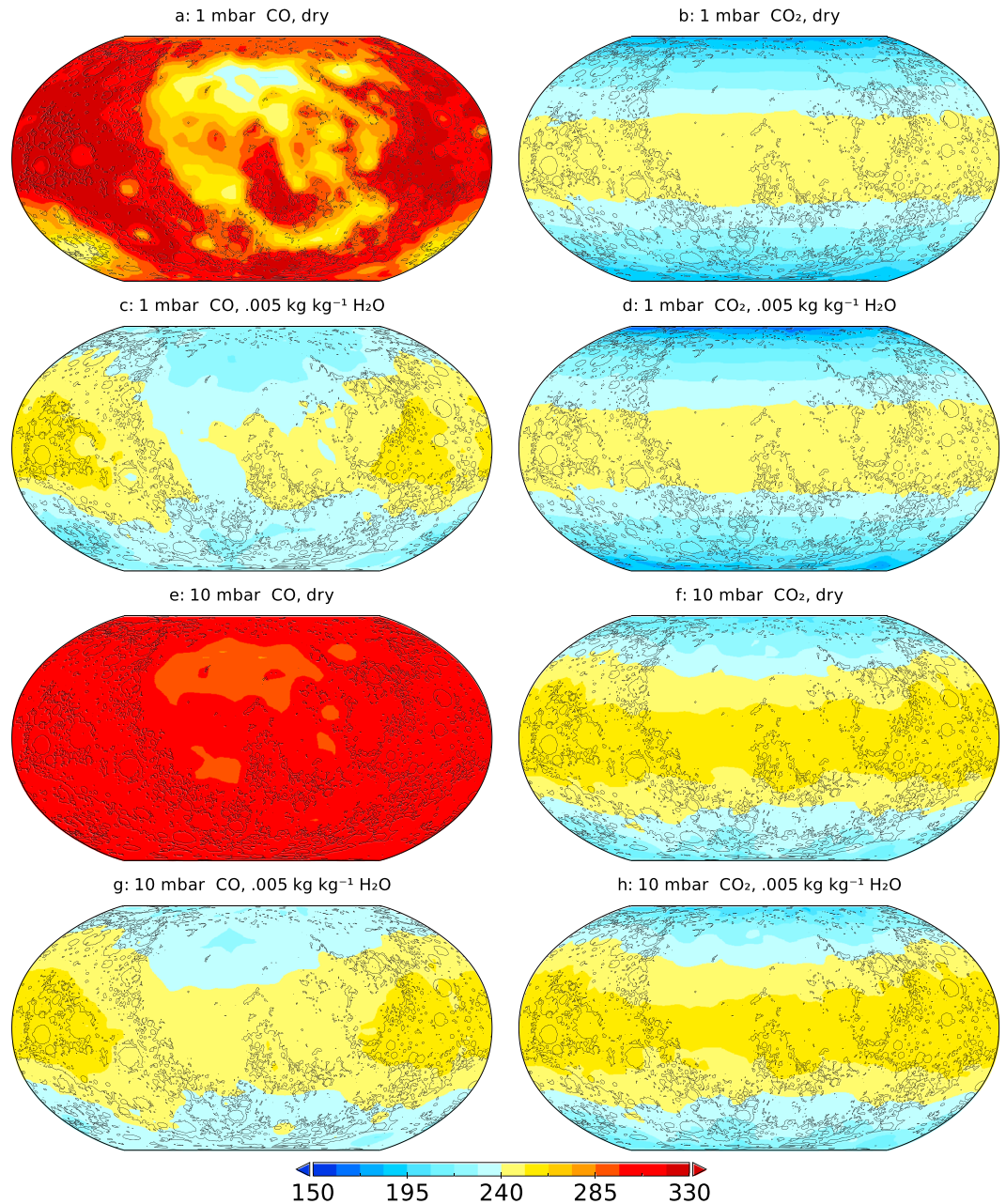| Number	Distance from Earth (Earth radii)	Rotation period (days)	Obliquity to Sun (°)	Atmospheric composition	Surface pressure (mbar)	Initial H_2O (kg/kg atmosphere)
1a, 1b, 1c	45	17.8	0	100% CO	10, 2.5, 1	10^{-7}
2a, 2b, 2c	45	17.8	0	100% CO_2	10, 2.5, 1	10^{-7}
3a, 3b, 3c	45	17.8	0	100% CO	10, 2.5, 1	5×10^{-3}
4a, 4b, 4c	45	17.8	0	100% CO_2	10, 2.5, 1	5×10^{-3}

4.3. Experiments

We conducted experiments for 10-, 2.5-, and 1-mbar atmosphere as shown in Table 2. They represent the limiting cases for the lunar atmosphere 3.5 Ga as was discussed in previous sections. In all cases the simulations were run until the model reached an equilibrium state, which for a cool dry terrestrial world happens relatively quickly (on the order of 10–20 simulation years). We considered cases of "dry" and "wet" atmospheres. In the former case the atmosphere was initialized with 10^{-7} kg H_2O per kilogram of atmosphere and stayed close to this humidity level throughout the simulations. In the latter case it was initialized to 5×10^{-3} kg/kg (except for the upper 10% of the atmosphere, where it was initialized to 0) and evolved to equilibrium together with the rest of the system. One should notice that here we are talking about the meteorological equilibrium. Some amount of water is being lost due to continuous freezing out at the poles and in permanently shadowed regions. But these are very slow processes (once the initial water has settled as frost in polar regions and deep in the soil elsewhere, there is very little supply to the atmosphere), which happen on geological rather than meteorological scales and compete with water delivery by volcanic outgassing and impactors. It is beyond the scope of this work to consider such processes.

5. Results and Discussion

The distinctive property of a climate on a slowly rotating planet with a thin atmosphere is a very strong diurnal cycle. In all our experiments the typical ground temperature at night was ∼200 K, while during the day at the substellar point it was as high as ∼340 K. Figures S3–S5 (supporting information) show instantaneous maps of ground temperature, lower atmosphere temperature, and surface pressure for 1-mbar experiments. While in the CO_2 case the atmospheric temperature basically follows the ground temperature, the CO case is more complicated, with more uniform temperatures over the surface and the effect of topography more pronounced. We discuss this in more detail below, when we look at Figure 1. Despite cold temperatures during the lunar night, in all our experiments a diurnal cycle ensures that any water cold-trapped on the night side only remains there temporarily. Permanent cold trapping is only possible at the poles, where the temperatures remain consistently cold.

Figures 1a–1d show maps of annually averaged air temperature of the lowest atmospheric layer (constituting 2% of the entire atmospheric mass) for the 1-mbar GCM simulations presented in Table 2. Of particular interest is to compare Figures 1a and 1b, which correspond to CO and CO_2 atmospheres on a dry planet. At first glance the results seem to be counterintuitive as the greenhouse gas-dominated atmosphere (CO_2) is for the most part cooler than the radiatively neutral (CO) atmosphere. This happens not only at the surface but throughout the entire depth of the atmosphere. The average bulk atmospheric temperature is 211.3 K for the CO_2 atmosphere and 281 K for the CO atmosphere. The explanation comes from the fact that in the case of a slowly rotating planet with such a thin atmosphere a significant amount of atmospheric heating is received from the ground through turbulent heat flux during the daytime when the ground is hot. During the nighttime the ground cools quickly through radiative cooling which leads to stable stratification of the planetary boundary layer and effective suppression of turbulent exchange fluxes between the ground and atmosphere. So the only possibility for the atmosphere to cool during the nighttime is through radiative cooling. But a radiatively neutral CO atmosphere cannot radiatively cool, basically preserving the energy obtained from the ground during the daytime and staying warmer than the CO_2-dominated "greenhouse" atmosphere.

a: 1 mbar CO, dry

b: 1 mbar CO_2, dry

c: 1 mbar CO, .005 kg kg^{-1} H_2O

d: 1 mbar CO_2, .005 kg kg^{-1} H_2O

e: 10 mbar CO, dry

f: 10 mbar CO_2, dry

g: 10 mbar CO, .005 kg kg^{-1} H_2O

h: 10 mbar CO_2, .005 kg kg^{-1} H_2O

150   195   240   285   330

Figure 1. Lower atmospheric layer (2% mass) temperature (K) for a pure CO (left) and a pure CO_2 (right) 1-mbar (a–d) and 10-mbar (e–h) atmosphere. The first row represents the experiments with a dry atmosphere (experiments 1c and 2c in Table 2). The second row corresponds to experiments that were initialized with 0.005 kg H_2O per kilogram of atmosphere (experiments 3c and 4c in Table 2). The experiments in the third and fourth rows are similar to the ones in the top rows, except that they correspond to 10-mbar atmosphere (experiments 1a, 2a, 3a, and 4a in Table 2).

When one adds small amounts of water to the system, as we have done in the experiments in Figures 1c and 1d, the CO-dominated atmosphere is no longer radiatively neutral (water vapor being a greenhouse gas), and the results become more conventional. While adding water has very little effect on the CO_2-dominated atmosphere (the bulk temperature increased slightly to 216 K), in the CO case the surface air temperature and the entire atmosphere become much colder, with average bulk atmospheric temperature being 225.9 K.

The average equilibrium amount of water in the lower atmosphere was 6×10^{-4} and 1×10^{-4} kg/kg in CO and CO_2 1 mbar wet experiments, respectively. Though water content was higher in the CO atmosphere, we found that its sequestration rate to PSRs was lower as a result of extremely stable stratification due to much
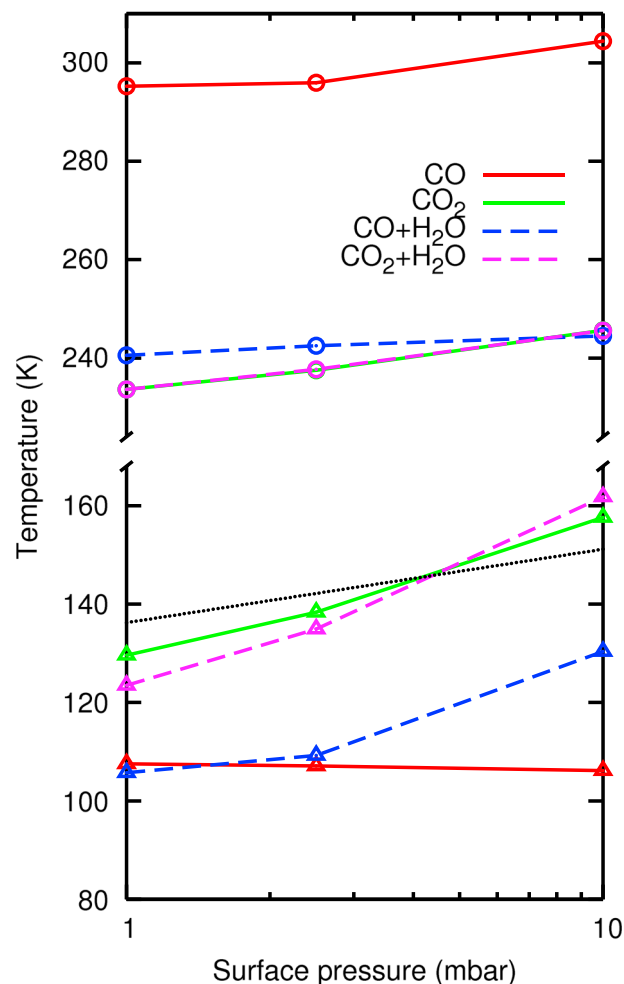
Figure 2. Global mean temperature of the lower layer (2% mass) of the atmosphere (circles) and ground temperature at the poles (triangles) as a function of atmospheric thickness. The marks show the results of experiments for 1-, 2.5-, and 10-mbar atmosphere. Black dotted line represents the CO_2 condensation curve.

lower temperatures inside the PSRs (Figure S2). Such low PSR temperatures in the CO case are due to the lack of greenhouse heating present in the CO_2 atmosphere.

Figures 1e–1h show temperature maps for the 10-mbar atmospheres. While most of these experiments exhibit similar behavior to the 1-mbar case, the dry CO atmosphere shows a more even distribution of temperature, most likely due to reduced topographic effect (the relative surface pressure difference between low and high altitude is lower for a thicker atmosphere.

Figure 2 presents the global average temperature of the first atmospheric layer for all 12 experiments listed in Table 2 (marked by circles). As in the 1-mbar case, the CO_2 dominated atmosphere dry and wet experiments basically coincide, while for the CO atmosphere they are separated by ∼50 K. In all experiments the temperature increases as the atmosphere gets thicker, due to the increased greenhouse effect and more efficient turbulent transfer of the heat from the surface. One should notice that in all cases the average atmospheric temperature is much warmer than the threshold discussed in section 2, so provided that one has a sufficient water supply it is likely that the atmosphere would be CO_2-dominated.

Figure 2 also presents the ground (regolith) temperature at the north pole (those experiments are marked with triangles). This is the coldest temperature at the surface of the Moon outside the PSRs. As one would expect, this temperature also increases with increasing atmospheric thickness (due to the greenhouse effect), except for the case of the dry CO atmosphere, which is radiatively neutral (the slight negative trend is due to increased Rayleigh scattering in thicker atmospheres). One important fact to notice is that the lines rep-

resenting the experiments with a CO_2-dominated atmosphere cross the CO_2 condensation threshold (black dotted line). Hence, for surface pressures of 2.5 mbar and lower such an atmosphere is prone to collapse, condensing at the poles. Condensation will be even more intense inside PSRs. Our estimates give that the 1-mbar CO_2-dominated atmosphere will lose about 0.01 of its mass per year due to condensation around the poles and in PSRs. The CO-dominated atmosphere does not have this problem, since the CO condensation temperature is much lower ($\sim$50 K at 1-mbar pressure). Extremely cold temperatures at the poles are partially a consequence of the zero obliquity used. If the Moon had a substantial obliquity at the epoch modeled herein it could warm the poles and mitigate the problem of a potential collapse of the CO_2-dominated atmosphere.

The past outgassing rates from lunar maria are a subject of active research and are still poorly constrained. In this work we used typical atmospheric pressures which would result from the relatively high outgassing rates conjectured by NK2017. In the future we plan to consider thinner atmospheres, which would result from lower outgassing rates proposed in other research. More work can be done to estimate atmospheric escape rates by simulating a realistic upper atmosphere. This could lead to the estimation of an additional deuteration in the water potentially deposited at the poles, which would be a way to confirm the existence of this past atmosphere.

References

Airapetian, V., Glocer, A., & Gronoff, G. (2015). The early Earth under a superflare and super-CME attack: Prospects for life. *Proceedings of the International Astronomical Union*, *11*(S320), 409–415.

Airapetian, V., Glocer, A., Gronoff, G., Hébrard, E., & Danchi, W. (2016). Prebiotic chemistry and atmospheric warming of early Earth by an active young Sun. *Nature Geoscience*, *9*(6), 452.

Airapetian, V. S., Glocer, A., Khazanov, G. V., Loyd, R. O. P., France, K., Sojka, J., et al. (2017). How hospitable are space weather affected habitable zones? The role of ion escape. *The Astrophysical Journal Letters*, *836*(1), L3.

Barker, M. K., Mazarico, E., Neumann, G. A., Zuber, M. T., Haruyama, J., & Smith, D. E. (2016). A new lunar digital elevation model from the lunar orbiter laser altimeter and SELENE Terrain Camera. *Icarus*, *273*, 346–355. https://doi.org/10.1016/j.icarus.2015.07.039

Benna, M., Mahaffy, P. R., Halekas, J. S., Elphic, R. C., & Delory, G. T. (2015). Variability of helium, neon, and argon in the lunar exosphere as observed by the LADEE NMS instrument. *Geophysical Research Letters*, *42*, 3723–3729. https://doi.org/10.1002/2015GL064120

Buratti, B. J., Hillier, J. K., & Wang, M. (1996). The lunar opposition surge: Observations by Clementine. *Icarus*, *124*(2), 490–499. https://doi.org/10.1006/icar.1996.0225

Canup, R. M. (2004). Dynamics of lunar formation. *Annual Review of Astronomy and Astrophysics*, *42*, 441–475. https://doi.org/10.1146/annurev.astro.41.082201.113457

Catling, D. C., & Kasting, J. F. (2017). *Atmospheric evolution on inhabited and lifeless worlds*. Cambridge: Cambridge University Press.

Claire, M. W., Sheets, J., Cohen, M., Ribas, I., Meadows, V. S., & Catling, D. C. (2012). The evolution of solar flux from 0.1 nm to 160 μm: Quantitative estimates for planetary studies. *The Astrophysical Journal*, *757*(1), 95.

Cook, J. C., Stern, S. A., Feldman, P. D., Gladstone, G. R., Retherford, K. D., & Tsang, C. C. C. (2013). New upper limits on numerous atmospheric species in the native lunar atmosphere. *Icarus*, *225*(1), 681–687. https://doi.org/10.1016/j.icarus.2013.04.010

Crotts, A. (2014). *The new Moon: Water, exploration, and future habitation*. Cambridge: Cambridge University Press. https://books.google.se/books?id=a0pCBAAAQBAJ

Ćuk, M., Hamilton, D. P., Lock, S. J., & Stewart, S. T. (2016). Tidal evolution of the Moon from a high-obliquity, high-angular-momentum Earth. *Nature*, *539*, 402–406. https://doi.org/10.1038/nature19846

Elkins-Tanton, L. T., Burgess, S., & Yin, Q.-Z. (2011). The lunar magma ocean: Reconciling the solidification process with lunar petrology and geochronology. *Earth and Planetary Science Letters*, *304*(3-4), 326–336.

Erkaev, N. V., Lammer, H., Odert, P., Kulikov, Y. N., Kislyakova, K. G., Khodachenko, M. L., et al. (2013). XUV-exposed, non-hydrostatic hydrogen-rich upper atmospheres of terrestrial planets. Part I: Atmospheric expansion and thermal escape. *Astrobiology*, *13*(11), 1011–1029.

Fahr, H. J., & Shizgal, B. (1983). Modern exospheric theories and their observational relevance. *Reviews of Geophysics*, *21*(1), 75–124. https://doi.org/10.1029/RG021i001p00075

Gao, P., Hu, R., Robinson, T. D., Li, C., & Yung, Y. L. (2015). Stability of CO_2 atmospheres on desiccated M dwarf exoplanets. *The Astrophysical Journal*, *806*(2), 249.

Garcia-Sage, K., Glocer, A., Drake, J. J., Gronoff, G., & Cohen, O. (2017). On the magnetic protection of the atmosphere of Proxima Centauri b. *The Astrophysical Journal Letters*, *844*, L13. https://doi.org/10.3847/2041-8213/aa7eca

Gronoff, G., Rahmati, A., Wedlund, C. S., Mertens, C. J., Cravens, T. E., & Kallio, E. (2014). The precipitation of keV energetic oxygen ions at Mars and their effects during the comet Siding Spring approach. *Geophysical Research Letters*, *41*, 4844–4850. https://doi.org/10.1002/2014GL060902

Gronoff, G., Simon Wedlund, C., Mertens, C. J., Barthélemy, M., Lillis, R. J., & Witasse, O. (2012). Computing uncertainties in ionosphere-airglow models: II. The Martian airglow. *Journal of Geophysical Research*, *117*, A05309. https://doi.org/10.1029/2011JA017308

Gronoff, G., Simon Wedlund, C., Mertens, C. J., & Lillis, R. J. (2012). Computing uncertainties in ionosphere-airglow models: I. Electron flux and species production uncertainties for Mars. *Journal of Geophysical Research*, *117*, A04306. https://doi.org/10.1029/2011JA016930

Halliday, A. N. (2008). A young Moon-forming giant impact at 70–110 million years accompanied by late-stage mixing, core formation and degassing of the Earth. *Philosophical Transactions of the Royal Society of London A: Mathematical, Physical and Engineering Sciences*, *366*(1883), 4163–4181. https://doi.org/10.1098/rsta.2008.0209

Harman, C., Pavlov, A., Babikov, D., & Kasting, J. (2018). Chain formation as a mechanism for mass-independent fractionation of sulfur isotopes in the Archean atmosphere. *Earth and Planetary Science Letters*, *496*, 238–247.

Harman, C., Schwieterman, E., Schottelkotte, J. C., & Kasting, J. (2015). Abiotic O_2 levels on planets around F, G, K, and M stars: Possible false positives for life? *The Astrophysical Journal*, *812*(2), 137.

Hartmann, W. K., & Davis, D. R. (1975). Satellite-sized planetesimals and lunar origin. *Icarus*, *24*(4), 504–515. https://doi.org/10.1016/0019-1035(75)90070-6

Herwartz, D., Pack, A., Friedrichs, B., & Bischoff A. (2014). Identification of the giant impactor Theia in lunar rocks. *Science*, *344*(6188), 1146–1150. https://doi.org/10.1126/science.1251117

Hunten, D. M. (1973). The escape of light gases from planetary atmospheres. *Journal of the Atmospheric Sciences*, *30*(8), 1481–1494.

Hunten, D. M. (1982). Thermal and nonthermal escape mechanisms for terrestrial bodies. *Planetary and Space Science*, *30*(8), 773–783.

Kasting, J. F., Zahnle, K., Pinto, J., & Young, A. (1989). Sulfur, ultraviolet radiation, and the early evolution of life. *Origins of Life and Evolution of the Bio-sphere*, *19*(2), 95–108.

Kislyakova, K. G., Lammer, H., Holmström, M., Panchenko, M., Odert, P., Erkaev, N. V., et al. (2013). XUV-exposed, non-hydrostatic hydrogen-rich upper atmospheres of terrestrial planets. Part II: Hydrogen coronae and ion escape. *Astrobiology*, *13*(11), 1030–1048.

Koga, R., Tsuchiya, F., Kagitani, M., Sakanoi, T., Yoneda, M., Yoshioka, K., et al. (2018). Spatial distribution of Io's neutral oxygen cloud observed by Hisaki. *Journal of Geophysical Research: Space Physics*, *123*, 3764–3776. https://doi.org/10.1029/2018JA025328

Kulikov, Y. N., Lammer, H., Lichtenegger, H. I., Penz, T., Breuer, D., Spohn, T., et al. (2007). A comparative study of the influence of the active young Sun on the early atmospheres of Earth, Venus, and Mars, *Geology and habitability of terrestrial planets* (pp. 207–243). New York: Springer.

Kulikov, Y. N., Lammer, H., Lichtenegger, H., Terada, N., Ribas, I., Kolb, C., et al. (2006). Atmospheric and water loss from early Venus. *Planetary and Space Science*, *54*(13-14), 1425–1444.

Lock, S. J., & Stewart, S. T. (2016). The structure of terrestrial bodies: Impact heating, corotation limits, and synestias. *Journal of Geophysical Research: Planets*, *122*, 950–982. https://doi.org/10.1002/2016JE005239

Lock, S. J., Stewart, S. T., Petaev, M. I., Leinhardt, Z., Mace, M. T., Jacobsen, S. B., & Cuk, M. (2017). The origin of the Moon within a terrestrial synestia. *Journal of Geophysical Research: Planets*, *123*, 910–951. https://doi.org/10.1002/2017JE005333

Lucey, P. G., Neumann, G. A., Riner, M. A., Mazarico, E., Smith, D. E., Zuber, M. T., et al. (2014). The global albedo of the Moon at 1064 nm from LOLA. *Journal of Geophysical Research: Planets*, *119*, 1665–1679. https://doi.org/10.1002/2013JE004592

Lyons, J. R. (2008). An estimate of the equilibrium speciation of sulfur vapor over solid sulfur and implications for planetary atmospheres. *Journal of Sulfur Chemistry*, *29*(3-4), 269–279.

Mazarico, E., Neumann, G., Smith, D., Zuber, M., & Torrence, M. (2011). Illumination conditions of the lunar polar regions using LOLA topography. *Icarus*, *211*(2), 1066–1081. https://doi.org/10.1016/j.icarus.2010.10.030

Needham, D. H., & Kring, D. A. (2017). Lunar volcanism produced a transient atmosphere around the ancient Moon. *Earth and Planetary Science Letters*, *478*, 175–178.

Nemchin, A., Timms, N., Pidgeon, R., Geisler, T., Reddy, S., & Meyer, C. (2009). Timing of crystallization of the lunar magma ocean constrained by the oldest zircon. *Nature Geoscience*, *2*(2), 133.

Prem, P., Artemieva, N. A., Goldstein, D. B., Varghese, P. L., & Trafton, L. M. (2015). Transport of water in a transient impact-generated lunar atmosphere. *Icarus*, *255*, 148–158. https://doi.org/10.1016/j.icarus.2014.10.017

Renggli, C., King, P., Henley, R., & Norman, M. (2017). Volcanic gas composition, metal dispersion and deposition during explosive volcanic eruptions on the Moon. *Geochimica et Cosmochimica Acta*, *206*, 296–311.

Rufu, R., Aharonson, O., & Perets, H. B. (2017). A multiple-impact origin for the Moon. *Nature Geoscience*, *10*(2), 89–94.

Saxena, P., Elkins-Tanton, L., Petro, N., & Mandell, A. (2017). A model of the primordial lunar atmosphere. *Earth and Planetary Science Letters*, *474*, 198–205. https://doi.org/10.1016/j.epsl.2017.06.031

Schmidt, G. A., Kelley, M., Nazarenko, L., Ruedy, R., Russell, G. L., Aleinov, I., et al. (2014). Configuration and assessment of the GISS ModelE2 contributions to the CMIP5 archive. *Journal of Advances in Modeling Earth Systems*, *6*, 141–184. https://doi.org/10.1002/2013MS000265

Siegler, M. A., Bills, B. G., & Paige, D. A. (2011). Effects of orbital evolution on lunar ice stability. *Journal of Geophysical Research*, *116*, E03010. https://doi.org/10.1029/2010JE003652

Siegler, M., Paige, D., Williams, J.-P., & Bills, B. (2015). Evolution of lunar polar ice stability. *Icarus*, *255*, 78–87. https://doi.org/10.1016/j.icarus.2014.09.037

Stern, S. A. (1999). The lunar atmosphere: History, status, current problems, and context. *Reviews of Geophysics*, *37*, 453–492. https://doi.org/10.1029/1999RG900005

Stewart, B. D., Pierazzo, E., Goldstein, D. B., Varghese, P. L., & Trafton, L. M. (2011). Simulations of a comet impact on the Moon and associated ice deposition in polar cold traps. *Icarus*, *215*(1), 1–16. https://doi.org/10.1016/j.icarus.2011.03.014

Tian, F., Kasting, J. F., & Solomon, S. C. (2009). Thermal escape of carbon from the early Martian atmosphere. *Geophysical Research Letters*, *36*, L02205. https://doi.org/10.1029/2008GL036513

Tikoo, S. M., Weiss, B. P., Shuster, D. L., Suavet, C., Wang, H., & Grove, T. L. (2017). A two-billion-year history for the lunar dynamo. *Science Advances*, *3*(8), e1700207. https://doi.org/10.1126/sciadv.1700207

Volkov, A. N., Johnson, R. E., Tucker, O. J., & Erwin, J. T. (2011). Thermally driven atmospheric escape: Transition from hydrodynamic to Jeans escape. *The Astrophysical Journal Letters*, *729*(2), L24.

Vondrak, R. R. (1974). Creation of an artificial lunar atmosphere. *Nature*, *248*(5450), 657.

Vondrak, R. R. (1992). Lunar base activities and the lunar environment. In W. W. Mendell (Ed.), *Lunar bases and space activities of the 21st century* (pp. 337–345). Washington: NASA.

Vondrak, R. R., Freeman, J. W., & Lindeman, R. (1974). Measurements of lunar atmospheric loss rate, *Lunar and planetary science conference proceedings* (Vol. 5, pp. 2945–2954). New York: Pergamon Press.

Ward, W. R. (1975). Past orientation of the lunar spin axis. *Science*, *189*, 377–379. https://doi.org/10.1126/science.189.4200.377

Way, M. J., Aleinov, I., Amundsen, D. S., Chandler, M. A., Clune, T. L., Del Genio, A. D., et al. (2017). Resolving Orbital and Climate Keys of Earth and Extraterrestrial Environments with Dynamics (ROCKE-3D) 1.0: A general circulation model for simulating the climates of rocky planets. *Astrophysical Journal, Supplement Series*, *231*, 12. https://doi.org/10.3847/1538-4365/aa7a06

Webb, D. (1982). Tides and the evolution of the Earth–Moon system. *Geophysical Journal of the Royal Astronomical Society*, *70*(1), 261–271.

Williams, G. E. (1999). Geological constraints on the precambrian history of Earth's rotation and the Moon's orbit. *Reviews of Geophysics*, *38*(1), 37–59. https://doi.org/10.1029/1999RG900016

Zahnle, K. J., & Catling, D. C. (2017). The cosmic shoreline: The evidence that escape determines which planets have atmospheres, and what this may mean for Proxima Centauri b. *The Astrophysical Journal*, *843*(2), 122.

Zahnle, K. J., Haberle, R. M., Catling, D. C., & Kasting, J. F. (2008). Photochemical instability of the ancient Martian atmosphere. *Journal of Geophysical Research*, *113*, E11004. https://doi.org/10.1029/2008JE003160

Zahnle, K. J., Kasting, J. F., & Pollack, J. B. (1990). Mass fractionation of noble gases in diffusion-limited hydrodynamic hydrogen escape. *Icarus*, *84*(2), 502–527.

Zhang, M. H. G., Luhmann, J. G., Bougher, S. W., & Nagy, A. F. (1993). The ancient oxygen exosphere of Mars: Implications for atmosphere evolution. *Journal of Geophysical Research*, *98*(E6), 10,915–10,923. https://doi.org/10.1029/93JE00231

Zolotov, M. Y., & Fegley Jr, B. (1999). Oxidation state of volcanic gases and the interior of Io. *Icarus*, *141*(1), 40–52.